First results from electron beam experiments at FAST

Alex Halavanau (NIU advisor: P. Piot, FNAL advisor: C. Thangaraj)

Northern Illinois University/Fermilab

27 June 2016

Fermilab Accelerator Science and Technology facility (FAST)

The FAST facility comprises a 50-MeV injector followed by an accelerator cryomodule capable of boosting the beam energy up to 300 MeV.

Outline

- Transverse beam dynamics and trasport matrix measurement of a TESLA-type cavity
- Microlens array laser trasnverse shaping technique
- Magnetized beam experiments at FAST
- High energy beamline longitudinal space charge amplifier experiment
- Conclusions

Cavity transport matrix measurement

- Motivation
- Analytical model
- Simulation software model
- Beam alignment in the cavity
- Experimental setups
- Preliminary results
- Future planned experiments
- Conclusions

* FAST - Fermilab Accelerator Science and Technology facility

π-mode SW superconducting cavity

Motivation: Several proposed or operating accelerator facilities include standing-wave (SW) TESLA-type cavities, such as FAST, ILC, LCLS-II, PIP2 and etc. to accelerate electron, proton or muon beams.

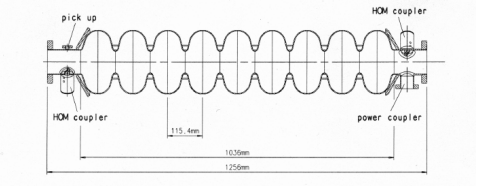

The transverse-focusing properties of such a cavity and non-ideal transverse-map effects introduced by field asymmetries in the vicinity of the input and high-order-mode radiofrequency (RF) couplers play a crucial role in transverse beam dynamics

1. Compare the experimental transverse transfer matrix with analytical model
2. Attempt to characterize the effects discussed above

Analytical model

The transfer matrix of a π-mode RF resonator was first derived by Chambers (1962) and generalized by Serafini and Rosenzweig (1994)

A particle in a standing wave field $E_z(z,t) = E_0 \sum_n a_n \cos(nkz)\sin(\omega t + \Delta\phi)$ experiences a ponderomotive-focusing force $F_r = -e(E_r - vB_\phi) \approx er\frac{\partial E_z}{\partial z}$. This yields the focusing strength $K_r = -\frac{(E_0 e)^2}{8(\gamma m)^2}$. The equation of motion then takes form:

$$x'' + \left(\frac{\gamma'}{\gamma}\right)x' + K_r\left(\frac{\gamma'}{\gamma}\right)^2 x = 0, \tag{1}$$

The solution of the Eq. 1 can be found in the form of $\mathbf{x}_f = R\mathbf{x}_i$, where the elements of 2×2 matrix R are (assuming ultra-relativistic beam and axially symmetric E-field):

$$\begin{aligned}
R_{11} &= \cos\alpha - \sqrt{2}\cos(\Delta\phi)\sin\alpha,\\
R_{12} &= \sqrt{8}\frac{\gamma_i}{\gamma'}\cos(\Delta\phi)\sin\alpha,\\
R_{21} &= -\frac{\gamma'}{\gamma_f}\left[\frac{\cos(\Delta\phi)}{\sqrt{2}} + \frac{1}{\sqrt{8}\cos(\Delta\phi)}\right]\sin\alpha,\\
R_{22} &= \frac{\gamma_i}{\gamma_f}[\cos\alpha + \sqrt{2}\cos(\Delta\phi)\sin\alpha],
\end{aligned} \tag{2}$$

where $\alpha \equiv \frac{1}{\sqrt{8}\cos(\Delta\phi)}\ln\frac{\gamma_f}{\gamma_i}$, and $\gamma_f \equiv \gamma_i + \gamma' z$ is the final Lorentz factor.

Simulation software model

1. **FAST injector contains two Tesla-type cavities**
2. IMPACT-T start-to-end model of FAST beamline was established
3. ASTRA model with HFSS 3D-field maps of the cavities was established

The difference between 1D and 3D simulations

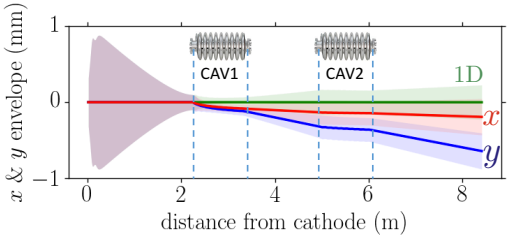

Beam steering by the cavities has been experimentally observed

Beam alignment in the cavities

Electron beam alignment in the cavities is very important for the performance of the beamline

The alignment is done in three steps

1. Manually send the beam through the cavity (0-th iteration)
2. Apply model dependent beam based alignment procedure to generate first set of trim values (work in progress by Sasha R.)
3. Apply conjugate gradient method that minimizes phase response of the cavity using BPM readouts (tested on quadrupoles and provided the alignment corrections that are being used at the moment; work in progress)
4. Verify the result by HOM signal from the cavities* (installation in progress)

*Assuming cavity was well aligned during the installation

3D field map simulation results

ASTRA simulations - study the effect of the noise in BPM with the beam RMS size σ

Conclusion: Instrumental error and orbit jitter can dramatically affect the results.

$\sigma = 1mm$

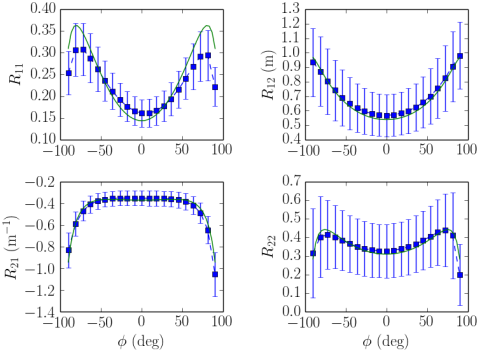

$\sigma = 0.1mm$

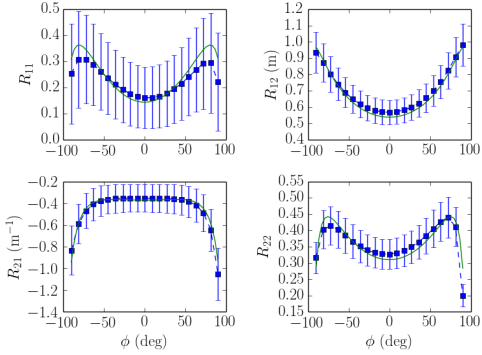

3D field map simulation results

ASTRA simulations - HOM coupler effects

Small coupling terms
(vary with energy/gradient)

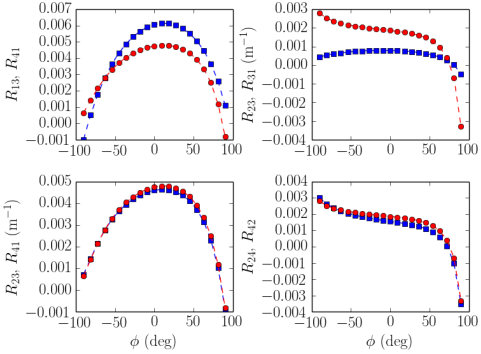

Matrix determinant
(agrees reasonably well)

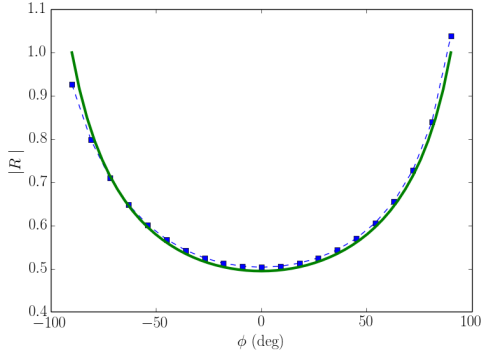

Improvement of the BPMs

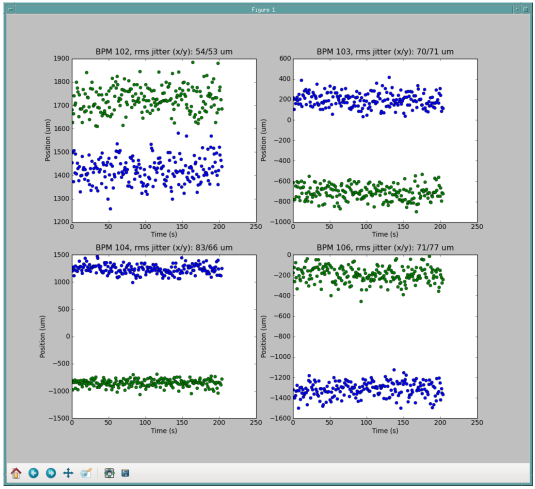

Improvements were made just a week ago!

Experimental setup (2015)

Schematics of the experiment

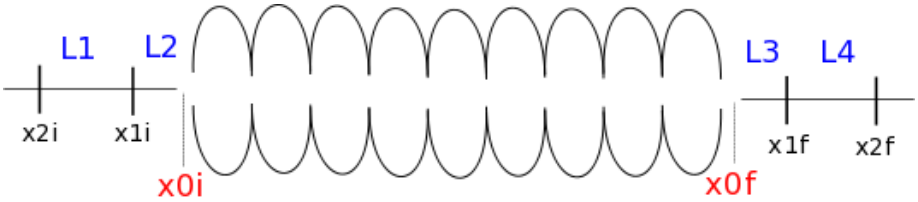

Advantages

1. Only one cavity with two BPMs upstream/downstream

Issues

1. Beam matching in CAV2 was not optimal; significant bunch lengthening in drift (where CAV1 now installed).
2. Geometric emittance was large (5 μm for a 200 pC beam)
3. Laser-phase instabilities hampered some of the measurements

Experimental setup (2016)

Schematics of the experiment

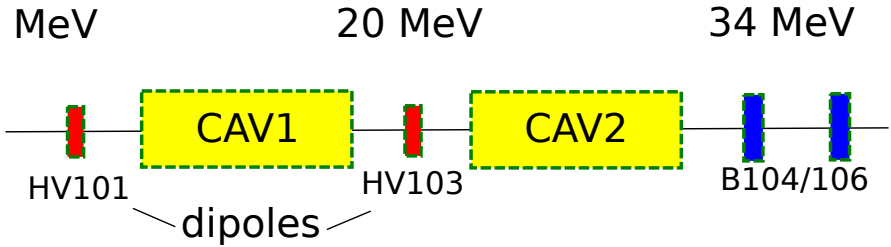

Advantages

1. Overall better laser performance
2. Improved instrumentation (BPM jitter < 80 um)

Issues

1. Strong focusing in CAV1 (need to lower the gradient)
2. CAV1 in place, need to adjust the beam size

First measurement campaign at FAST

800 orbits were recorded for 7 phase datapoints

Transverse coordinates were reconstructed as:

$$x_{0i/f} = x_{1i/f} \pm L_{2,3}/L_{1,4}(x_{1i/f} - x_{2i/f}), \qquad x'_{0i/f} = \pm(x_{1i/f} - x_{2i/f})/L_{1,4} \tag{3}$$

1. BPM nonlinear corrections were introduced in ACNET (by N. Eddy)
2. Developed measurement methods based on BPMs
3. Developed automated emittance measurement
4. Least-squares fitting code was implemented for data processing
5. Error bar estimation is made via bootstrap

Preliminary experimental results (2016)

Main diag. matrix elements

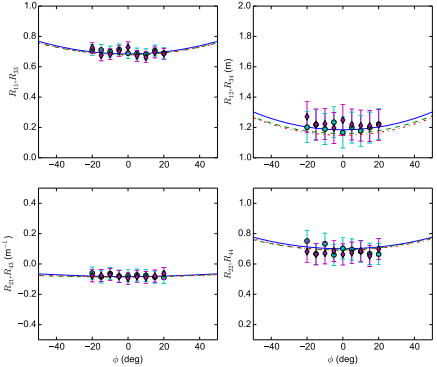

Off diag. matrix elements

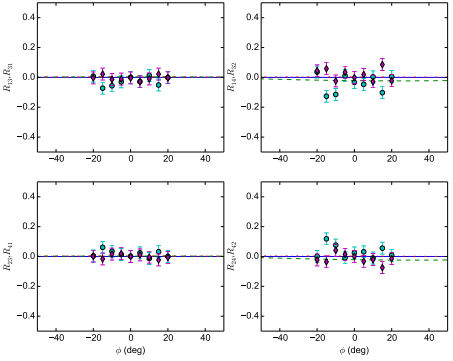

Matrix elements generally show agreement with theoretical (numerical) prediction

Preliminary experimental results

Matrix determinant

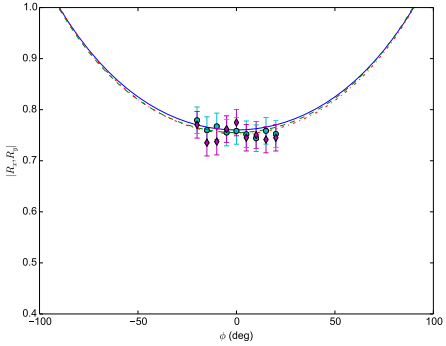

1. Results show good agreement with theory and simulations
2. Preliminary results were presented at IPAC16 (TUPMY038; Halavanau, A., et. al.)

Planned in 2016

1. Careful alignment in both CAV1/CAV2
2. More transport matrix measurements
3. Determinant damping study by reducing the gradient in CAV1
4. HOM steering effect study

Conclusions

1. Time dependent HOM coupler kick affects transverse beam dynamics at low energy (verified by both simulations and first experiments)
2. Understanding transverse beam dynamics in CAV1/CAV2 is important for successful FAST injector operation
3. FAST beamline has skew quadrupole magnets and could possibly correct for the HOM/Input coupler correlations (proposed for LCLS-II by D. Dowell)
4. New data was taken last Friday (work in progress)
5. Many developed complimentary tools and scripts are routinely reused in other experiments

Microlens experiment outline

- Motivation
- Microlens Array setup
- Optical transport design
- Initial laser tests at FAST facility
- Electron beam experiments at AWA facility
- First results and future planned experiments

* FAST - Fermilab Accelerator Science and Technology facility

** AWA - Argonne Wakefield Accelerator

Microlens arrays (MLAs)

Motivation: In photocathodes the achievable electron beam parameters are controlled by the laser used to trigger the photoemission. Non-ideal laser distribution hampers the final beam quality, and to overcome this, laser shaping methods are routinely employed.

Microlens arrays are fly-eye type light condensers

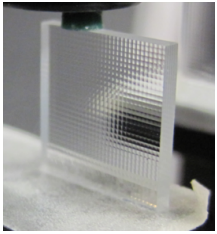

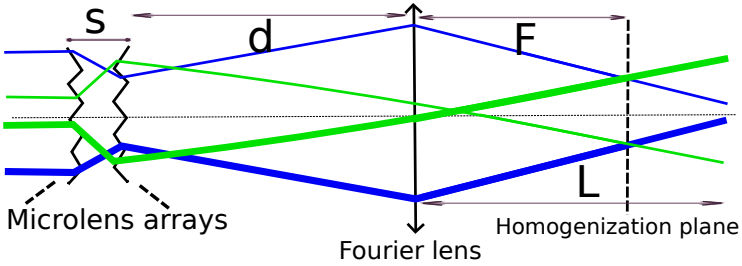

1. Produce uniform laser image in the focal plane of the mixing lens
2. Produce transversely modulated laser beams

Some useful expressions

We employed ABCD-model for the MLA setup. We find the diameter of the image at the homogenization plane to be:

$$D_h \approx \frac{Fp}{f^2}(2f - s)$$

It is also useful to estimate the required lens aperture:

$$A_F \approx \frac{dp}{f^2}(2f - s)$$

Practical implication may sometime result in $L \neq F$; then the size of the image is:

$$D \approx \frac{pL}{f^2}(2f - s) + \frac{dp(2f - s)}{f^2}\frac{F - L}{F}$$

Laser image analysis

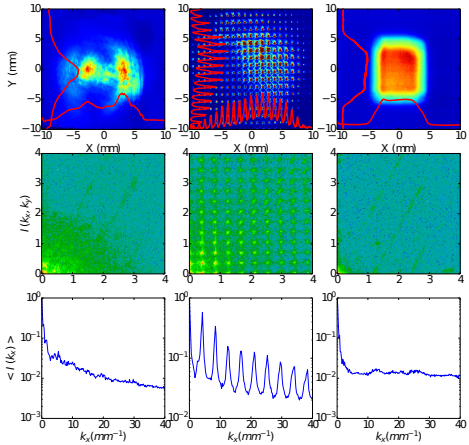

(left) Initial laser profile, (middle) patterned beam, (right) uniform beam

Transverse modulation for different MLA settings (low frequency modulation is dramatically improved!)

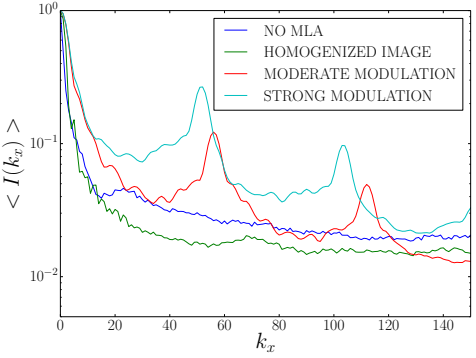

Optical transport design

1. Photocathodes often have long optical injection (limited by vacuum)
2. Require imaging solution (not 4F imaging)
3. Lens setup below can be further optimized (this is just a first trial)

Ray tracing of a five-lens transport capable of imaging the homogenized beam at the photocathode. The inset shows of a 8×8 array simulated using SRW.

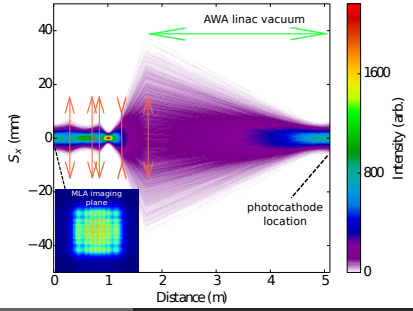

The schematics of the AWA linac (50 MeV) beamline

- Beam images were taken at low (8 MeV) and high (50 MeV) energy
- Various solenoid settings were tested to study the transport of patterned beams

*AWA - Argonne Wakefield Accelerator

Electron beam experiment

False color 8 MeV electron beam patterns for various matching solenoid current setting and charge. Left to right: Q=60pC, 80pC, 100pC, 120pC. Top to bottom: M=215A, 230A, 241A, 255A, 270A, 290A and BF=498A

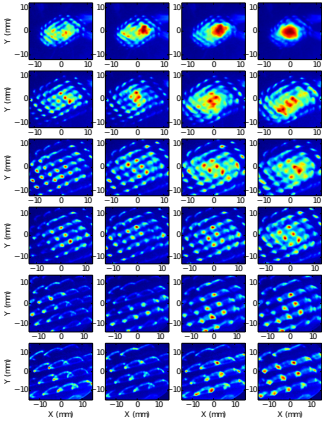

Bunching factor as a function of different solenoid settings for low energy beam

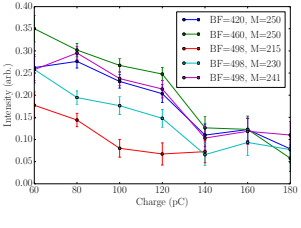

False color 50 MeV electron beam patterns for various charges. From left to right and top to bottom: Q=60pC, 100pC, 200pC, 300pC, 400pC, 500pC, 600pC, 700pC

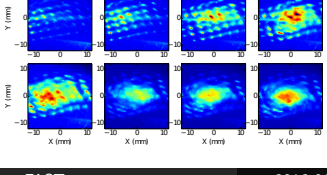

Conclusions

Applications of homogenized beams

1. Significantly improve the quality of the electron beam
2. Reduce transverse beam emittance by factor of 2 (verified with simulations and quadrupole scan measurements)

Applications of patterned beams

1. Provide an excellent beam based method for matching real machine parameters with simulation settings (work in progress)
2. Can be used in multiple THz radiation generation schemes (work in progress)
3. May be used as an alternative to slits in electron beam magnetization measurement (work in progress)

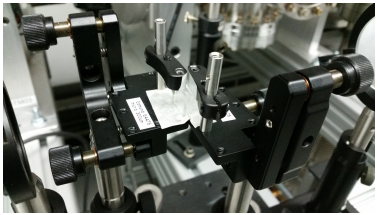

The results were recently reported at IPAC2016 (THPOW021, Halavanau, A., et. al.).

Existing and possible future collaborations

MLA is planned for installation at FAST

1. Argonne Wakefield Accelerator (AWA) facility
   (J. Power, E. Wisniewski, G. Ha, G. Qiang)
2. KEK facility (A. S. Aryshev)
3. ALS Accelerator Physics Group, LBNL (F. Sannibale)
4. SLAC (D. Ratner)

Motivation for magnetized beam experiments at FAST

1. Continue work pionereed at A0
2. Obtaining beams with high trasnverse emittance ratio (flat beams)
3. Current FAST optics has three quadrupoles to be skewed for flat beam production
4. Injection of the magnetized beams in IOTA (work in progress in collaboration with JLab)

CAM dominated beams

Total canonical angular momentum
of a charged particle in symmetric magnetic field is conserved

$$L = \gamma m r^2 \dot{\theta} + \frac{1}{2} e B_z(z) r^2 \tag{4}$$

The norm of $|\vec{L}|$ can be computed as $L = |\vec{r} \times \vec{p}| = x p_y - y p_x$.
The conservation of L immidieately yields that:

$$\frac{L}{\gamma m} = < \dot{\theta} r^2 > = \frac{\sigma_0^2 e B_{0z}}{2 \gamma m_e}, \tag{5}$$

where $< \dot{\theta} >$ is the time derivative of θ averaged over the distribution, B_{0z} is the field at the cathode, σ_0 is the RMS spot at the cathode and σ is the RMS beam size.
The particle total momentum $\vec{p} = p_r \hat{\mathbf{r}} + p_\theta \hat{\theta} + p_z \hat{\mathbf{z}}$ has non-zero $\hat{\theta}$-component $p_\theta = \gamma m_e r \dot{\theta}$ resulting in **CAM-dominated beam**.

CAM dominated beams

The envelope equation takes form:

$$\sigma'' - \frac{K}{4\sigma} - \frac{\epsilon_u^2}{\sigma^3} - \frac{\mathcal{L}^2}{\sigma^3} = 0, \tag{6}$$

where $K = 2I/I_0\gamma^3$ is the perveance, I and I_0 are the beam and Alfven current respectively, ϵ_u - geometric 4D emittance and magnetization $\mathcal{L} \equiv < L > /2\gamma mc$. When $\mathcal{L}$ is large - the beam is CAM dominated

Total 4D-emittance is conserved

$$det(J\Sigma - i\epsilon_{\pm} I) = 0, \tag{7}$$

where I and J are respectively unit and symplectic unit matrix.

Experimental setup

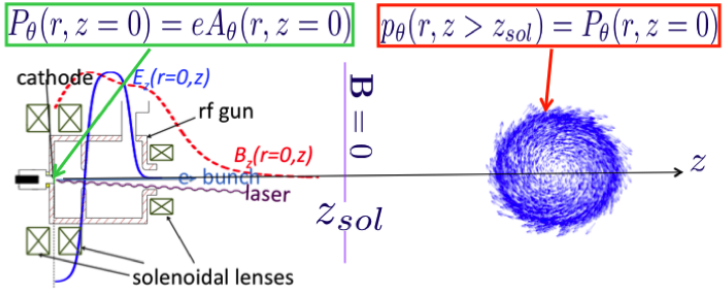

1. **FAST is capable of producing highly asymmetric beams** (verified with genetic algorithm optimization with IMPACT-T)
2. After round-to-flat transformation one of the emittances can be below thermal limit

Magnetization measurement experiment

1. Produce patterned beams via MLA laser shaping technique (red)
2. Adjust the solenoids to achieve magnetized state
3. Measure the rotation component (difference in the beam images) (green/blue)
4. Compare "mechanical" momentum to CAM

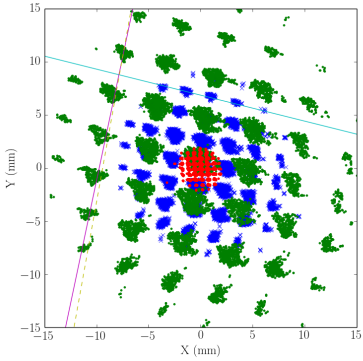

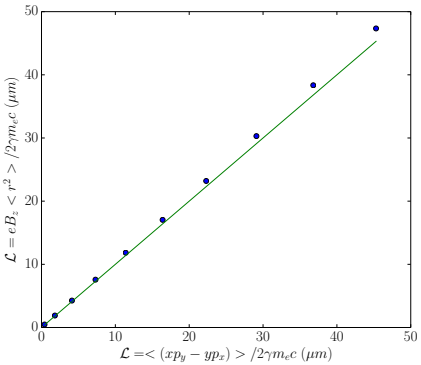

Conclusions

- Magnetized/flat beams at FAST have many potential applications
- FAST injector is capable of producing asymmetric beams ($\epsilon_x/\epsilon_y \approx 1000$)
- MLA setup at FAST can provide a diagnostic tool for magnetization measurement

LSCA: Motivation and goals

- Longitudinal space charge effects are responsible for unwanted energy modulations and emittance growth in FELs
- On the contrary, such instabilities were shown to be potentially useful for broadband coherent radiation generation*
- The technique was recently demonstrated in the optical domain**

- Study microbunching instabilities due to LSC in the chicane cascade
- Implement an efficient algorithm for 3D space charge force calculation
- Explore the possibility of the short wavelength radiation generation at FAST facility

*M. Dohlus, E. A. Schneidmiller, and M. V. Yurkov, *Phys. Rev. ST Accel. Beams*, **14**, *090702 (2011)*.
A. Marinelli, et al., *Phys. Rev. Lett.*, **110, *264802 (2013)*.

Space charge problem

- Many numerical and analytical methods "reduce" the space charge problem's complexity which ultimately limits the maximum attainable spatial resolution
- Most of the LSC studies use a simple 1D model based on impedance approximation
- Space charge problem is very similar to the well-known N-body problem in celestial mechanics
- Very effective algorithm for the gravitational N-body problem, so called "tree" or Barnes-Hut (BH) algorithm can be used*

Some conventional codes: ASTRA, SYNERGIA, TSTEP

*J. Barnes and P. Hut, *Nature*, **324**, *446 (1986)*.

Tree algorithm for SC-force calculation

- Scales as $\mathcal{O}(N \log N)$, where N is the number of macroparticles used to represent the beam
- Precision parameter corresponds to the "depth" of the tree
- Can be applied to many-body systems

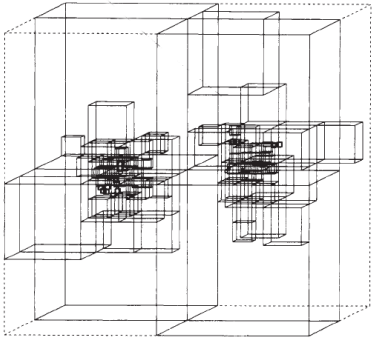

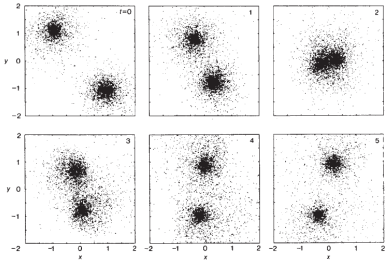

Images courtesy of J. Barnes

Procedure

- BH algorithm is used as an external script within the ELEGANT simulations.
- The distribution at the specified location was saved and Lorentz transformation to the bunch rest frame was applied.
- The BH algorithm was used to obtain the 3D electrostatic field $\mathbf{E}'$. This field was then transformed in the laboratory frame and the obtained electromagnetic fields $(\mathbf{E}, \mathbf{B})$ were used to compute the Lorentz force on each of the macroparticles composing the beam.
- The distribution then was finally passed back to ELEGANT and tracked up to the next space-charge kick where the above process repeated.
- We assumed no transverse motion in the bunch rest frame.
- We made no assumptions on the distribution and/or bunch shape.
- The BH algorithm will be a part of ELEGANT when fully tested.

Longitudinal space charge amplifier (LSCA)

- Can serve as addition to an existing FELs and linacs (use existing beamlines to generate powerful radiation)
- Can be used as a source of radiation with a relatively large bandwidth
- Can produce very short radiation pulses

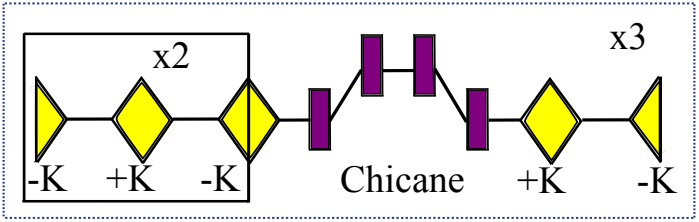

The yellow lozenges and purple rectangles respectively represent quadrupole and dipole magnets.

*M. Dohlus, E. A. Schneidmiller, and M. V. Yurkov, *Phys. Rev. ST Accel. Beams*, **14**, *090702 (2011)*.

LSCA cont.

The estimated gain per one chicane in LSCA is proportional to space-charge impedance $Z(k, r)$:

$$G_1 = Ck|R_{56}|\frac{I}{\gamma I_A}\frac{4\pi L_d|Z(k,r)|}{Z_0}\exp(-\frac{1}{2}C^2k^2R_{56}^2\sigma_\delta^2)$$

where R_{56} is the compressor longitudinal dispersion, σ_δ is the rms fractional energy spread, Ck is the modulation wavelength, and $Z_0 = 120\pi$ is the free-space impedance. The on-axis LSC impedance is given by:

$$Z(k) = -i\frac{Z_0}{\pi\gamma\sigma}\frac{\xi_\sigma}{4}e^{\xi_\sigma^2/2}\mathrm{Ei}(-\frac{\xi_\sigma^2}{2}), \quad \xi_\sigma = k\sigma/\gamma$$

*E.L. Saldin and E.A. Schneidmiller and M.V. Yurkov, *Nucl. Inst. and M. in Ph. R. Sec. A*, **483, 1-2, 2002**

*M. Venturini, *Phys. Rev. ST Accel. Beams*, **11**, *034401 (2008)*

LSCA cont.

To characterize the current (density) modulation one can introduce the bunching factor

$$b(\omega) = \frac{1}{N}|\sum_{n} \exp(-i\omega t_n)|$$

The broadband amplification process can be seen on the bunching factor curve as a broad peak. One can numerically compute the gain as:

$$G(\omega) = G_1 \times G_2 \times ... \times G_n = |\frac{b_f(\omega_f)}{b_0(\omega_i)}|$$

*JLAB-TN-14-016, Rui Li and C.-Y. Tsai

Validation

Let's consider initial bunch distribution with pre-modulated current profiles of the form $f(\mathbf{r}) = T(x, y)L_z(z)\,[1 + m\cos kz]$

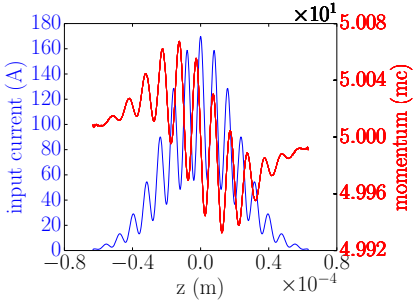

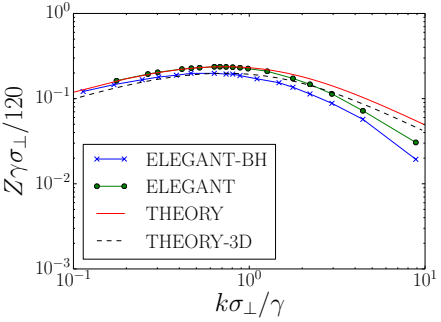

On the left: Initial density modulation resulted in energy modulation. *On the right:* The agreement between the BH algorithm and analytical impedance equation

$$Z(k) = -i\frac{Z_0}{\pi\gamma\sigma}\frac{\xi_\sigma}{4}e^{\xi_\sigma^2/2}\mathrm{Ei}(-\frac{\xi_\sigma^2}{2})$$

Bunching factor (averaged)

The LSC impedance results in selection of preferred frequency

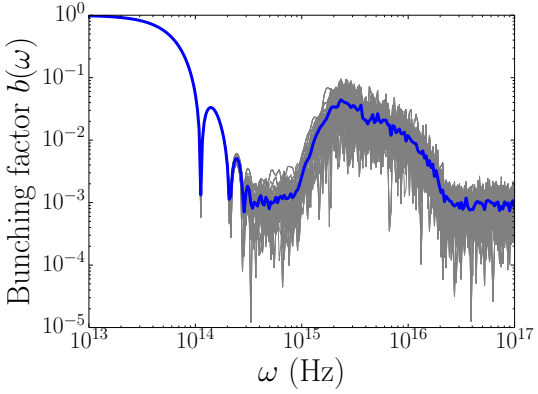

100 realizations with 1M particles (gray traces) and corresponding average (blue trace)

Simulations

- The simulations consider the lattice diagrammed below consisting of three LSCA modules each composed of three FODO cells with a chicane integrated in the last FODO cell.
- The BH code performs full 3D space-charge calculation and therefore inherits both transverse and longitudinal effects.
- All simulations were done for ($N = [0.1..4] \times 10^6$) particles to ensure the convergence and satisfying the statistical limit.

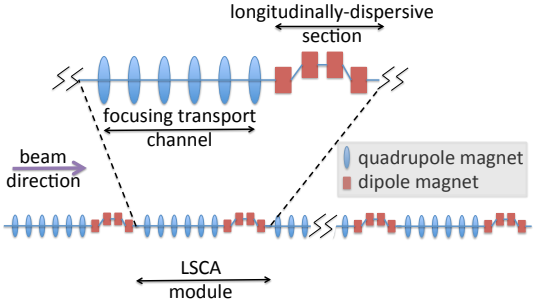

Energy scan

On the left: Bunching factor for different values of the chicane long. dispersion R_{56}

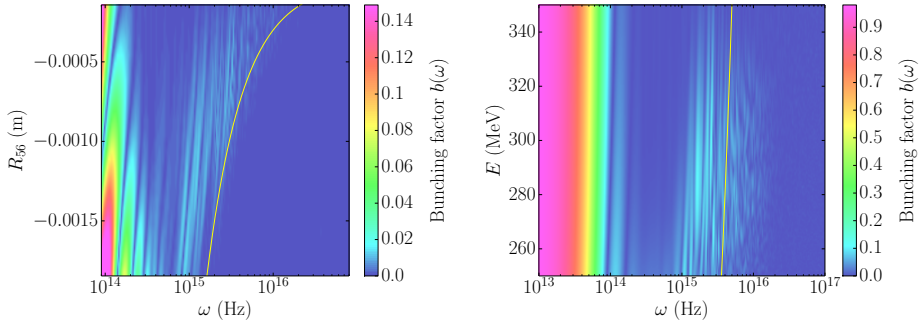

On the right: The change of the bunching factor vs energy of the bunch

Yellow solid line is analytical prediction.

More results: A. Halavanau and P. Piot, NIM A 2016 819 144-153.

Possible location at FAST

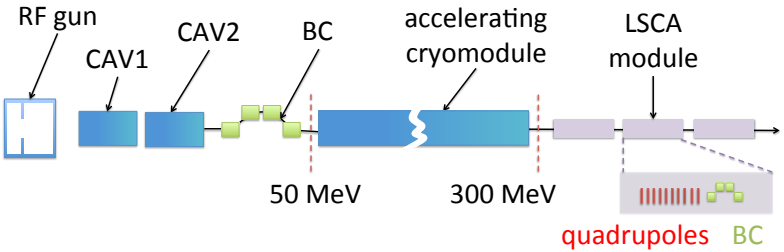

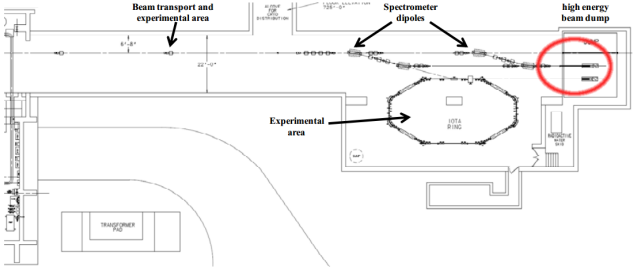

Possible use of the FAST beamline before the dump area

Desired bunch parameters

Parameter	Value	Units
Spotsize, σ	2.2 - 70.4	μm
Charge, Q	20.0	pC
Lorentz factor, γ	50 - 1000	–
Bunch duration, τ	120	fs
Norm. transv. emittance, $\varepsilon_{x,y}$	10^{-8}	m
Momentum spread, σ_δ	10^{-4}	–
Number of macroparticles, N	0.1 - 4	million
Total LSCA length, D	28.0	m

Possible LSCA at FAST

- Will not require much redesign of the lattice
- Can be compact (10-20 m)
- Can produce soft UV light. Still needs to be pushed for the VUV regime
- Local energy chirp can be made up-right to produce shorter pulses
- Some preliminary studies and discussion with collaborators at Jefferson Lab are on-going to check the possible use of IOTA to explore space charge microbunching instabilities relevant to electron-cooling ring for the electron-ion collider

Conclusions

- Using a gridless code adapted from Astrophysics we have investigated effects in the LSC impedance and found that the one-dimensional often used LSC impedance model is a good approximation.
- Nonetheless, our simulations consistently underestimate the analytical impedance over the range of k values explored. Such an effect was previously recognized and is attributed to the radial dependence of the LSC field conferring a similar dependence on the impedance.
- We demonstrated that LSCA can produce femtosecond pulses of light in optical regime.

Conclusions

- Adjusting the chicane parameter R_{56} can be a "single-knob" to generate light of a desired wavelength.
- The designed beamline at FAST facility allows proposed LSCA to be implemented and operate as a compact source of $100 - 1000$ nm light.
- It was shown that the LSCA can operate at various energies, what makes it possible to implement it at every FAST construction phase.

Credits

Acknowledgements:

- P. Piot (NIU, Fermilab) for supervising this research
- J. Power (ANL, AWA) and G. Ha (POSTECH) for their significant contribution to the MLA research
- A. Romanov (Fermilab) for his help with beam alignment at FAST and useful comments
- J. Barnes (U. Hawaii) for granting us use of his algorithm
- M. Borland (ANL) for his help and interest in including the algorithm into ELEGANT
- Rui Li (Jefferson Lab) and C.-Y. Tsai (Virginia Tech) for their interest and independent benchmarking of ELEGANT-BH

Thank you for your attention!

Backup slides

ELEGANT-BH vs LSCDRIFT

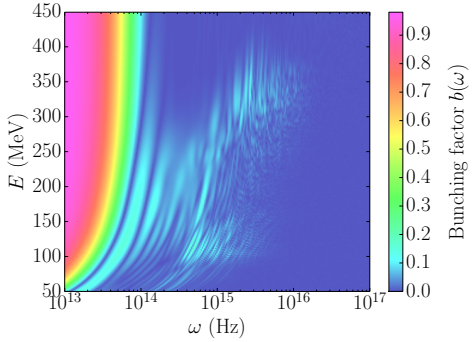

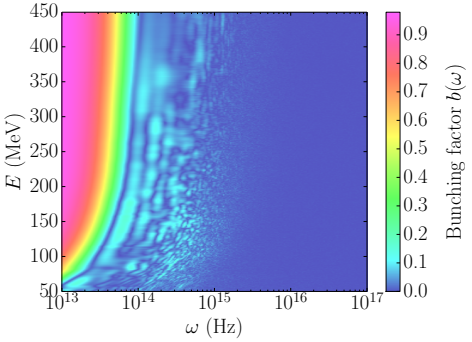

Softening

Potential estimator:

$$\Phi(x) = -k \sum_{i=1}^{N} \frac{m}{\epsilon} \phi(r) \left[\frac{|\vec{x} - \vec{x}_i|}{\epsilon} \right]$$

where $\phi(r)$ is the softening kernel and ϵ is the softening length.
The Plummer softening corresponds to:

$$\phi = (1 + r^2)^{-1/2}$$

Optimal choice of ϵ can reduce the bias in force calculation.

W. Dehnen, Mon. Not. R. Astron. Soc. 30 Nov 2000